

QUARK-NOVA REMNANTS IV: APPLICATION TO RADIO EMITTING AXP TRANSIENTS

RACHID OUYED, DENIS LEAHY AND BRIAN NIEBERGAL

Department of Physics and Astronomy, University of Calgary, 2500 University Drive NW, Calgary, Alberta, T2N 1N4 Canada
Draft version November 7, 2018

ABSTRACT

XTE J1810–197 and 1E 1547.0–5408 are two transient AXPs exhibiting radio emission with unusual properties. In addition, their spin down rates during outburst show opposite trends, which so far has no explanation. Here, we extend our quark-nova model for AXPs to include transient AXPs, in which the outbursts are caused by transient accretion events from a Keplerian (iron-rich) degenerate ring. For a ring with inner and outer radii of 23.5 km and 26.5 km, respectively, our model gives a good fit to the observed X-ray outburst from XTE J1810–197 and the behavior of temperature, luminosity, and area of the two X-ray blackbodies with time. The two blackbodies in our model are related to a heat front (i.e. Bohm diffusion front) propagating along the ring’s surface and an accretion hot spot on the quark star surface. Radio pulsations in our model are caused by dissipation at the light cylinder of magnetic bubbles, produced near the ring during the X-ray outburst. The delay between X-ray peak emission and radio emission in our model is related to the migration time of these bubbles to the light cylinder and scale with the period as $t_{\text{radio,delay}} \propto P^{7/2}$; we predict a ~ 2 year and ~ 1 month delay for XTE J1810–197 and 1E 1547.0–5408, respectively. We also estimate the total duration of the radio emission which we calculate to last for ~ 13 years and ~ 100 days for XTE J1810–197 and 1E 1547.0–5408, respectively. The observed flat spectrum, erratic pulse profile, and the pulse duration are all explained in our model as a result of X-point reconnection events induced by the dissipation of the bubbles at the light cylinder. The spin down rate of the central quark star can either increase or decrease depending on how the radial drift velocity of the magnetic islands changes with distance from the central star. We suggest an evolutionary connection between transient AXPs and typical AXPs in our model.

Subject headings: stars: evolution — stars: neutron: SGRs/AXPs — supernovae: SNR

1. INTRODUCTION

Anomalous X-ray pulsars (AXPs) are magnetars with rotation period of 2–12 seconds and inferred surface magnetic field strength $B \sim 10^{14-15}$ G (e.g. Woods & Thompson 2006; Kaspi 2007). In this work we focus on 2 AXPs, XTE J1810–197 and 1E 1547.0–5408, which are the only magnetars known to emit in the radio (Camilo et al. 2006). Both are demonstrably transient radio sources, having not been detected in previous surveys of adequate sensitivity. XTE J1810–197 is a transient AXP¹ first detected when its X-ray flux increased ~ 100 -fold compared to a quiescent level it maintained for at least 24 years (Ibrahim et al. 2004). Discovered with the *Einstein X-ray* satellite in 1980, 1E 1547.0–5408 was eventually identified as a magnetar candidate (Gelfand & Gaensler 2007) with spectral characteristics of an AXP. In this paper we look at these sources in the Quark-Nova context (hereafter QN; Ouyed et al. 2002) building on three previous papers where we explore its application to Soft Gamma-ray Repeaters (SGRs) (Ouyed, Leahy, & Niebergal 2007a; OLN1), to AXPs (Ouyed, Leahy, & Niebergal 2007b; OLN2), and to Rotating Radio Transients (RRATs) (Ouyed et al. 2008; OLN3), and super-luminous supernovae (Leahy&Ouyed 2008). But first, we briefly describe their observed X-ray and radio properties, during quiescence and bursting phases.

Electronic address: ouyed@phas.ucalgary.ca

¹ In the sense that in quiescence their surface temperature are as low as those of some ordinary young neutron stars

1.1. The X-ray emission

In the pre-burst era, XTE J1810–197’s ROSAT spectrum showed a single blackbody (BB) with temperature $T = 0.18$ keV, an emitting area of $\sim 520 \text{ km}^2 (d/3.3 \text{ kpc})^2$, and a luminosity of $L_{\text{BB}} \sim 5.6 \times 10^{33} \text{ erg s}^{-1} (d/3.3 \text{ kpc})^2$. During its bursting phase, XTE J1810–197 showed a hot blackbody ($T \sim 0.65$ keV) with an exponential decay in X-ray luminosity of ~ 280 days, as well as a warm blackbody ($T \sim 0.3$ keV) decaying at a rate of ~ 870 days (Gotthelf & Halpern 2007). For the case of 1E 1547.0–5408, after its radio detection (Camilo et al. 2007a), an X-ray outburst was confirmed (Halpern et al. 2008) with a record high luminosity of $\sim 1.7 \times 10^{35} (d/9.9 \text{ kpc})^2 \text{ erg s}^{-1}$ and with a total outburst energy of $10^{42} \text{ erg} < E_{\text{b}} < 10^{43} \text{ erg}$.

1.2. The radio emission

For XTE J1810–197, the radio emission began within 1 yr of its only known X-ray outburst (Camilo et al. 2006 and references therein). At its observed peak more than 3 yr after the X-ray outburst, the radio flux density was more than 50 times the pre-burst upper limit. The X-ray flux has since returned to its quiescent level nearly 4 yrs after the burst. 1E 1547.0–5408, although not as well sampled as XTE J1810–197, exhibits similar variations in flux density and was reported with a factor of 16 times the pre-burst upper limit (Camilo et al 2007a).

Trends in radio emission between the 2 sources can be summarized as follows:

- Both are very highly linearly polarized showing a flat spectrum over a wide range of frequencies. Their striking spectra (i.e. spectral index > -0.5) clearly distinguishable from ordinary radio pulsars (with a spectral index ~ -1.6 ; Camilo et al. 2007a&b).
- At their peak, both magnetars are very luminous in radio with luminosity at 1.4 GHz $L_{1.4} \geq 100\text{mJy (d/kpc)}^2$, which is larger than the $L_{1.4} \leq 2\text{mJy (d/kpc)}^2$ of most any ordinary young pulsar (e.g. Camilo et al. 2006). For XTE J1810–197, its assumed isotropic radio luminosity up to 42 GHz is about $2 \times 10^{30} \text{ erg s}^{-1}$ (Camilo et al. 2006).
- Both have variable pulse profiles (exhibiting sudden changes in radio pulse shape) and radio flux densities. The flux changes at all frequencies. At a given frequency there is no stable average pulse profile. Different pulse components change in relative intensity and new components sometimes appear. Sub-pulses with typical width approximately < 10 ms are observed (Camilo et al. 2007a&b).
- For XTE J1810–197, the torque was decreasing, at a time when the star was returning to quiescence years after the large outburst. As the torque decreased, so did the radio flux (Camilo et al. 2007b).
- In 1E 1547.0–5408, in contrast, the torque has been increasing, at a time when the X-ray flux has been gradually decreasing (Camilo et al. 2007a).

In this paper we extend our existing quark star model for AXPs to account for the observed behavior of these two transients. This paper is structured as follows: Section 2 gives the basic elements of the model. Section 3 describes the quiescent phase. Section 4, the bursting phase. Section 5, the radio emission. Model predictions are highlighted in Section 6 before we conclude in Section 7.

2. BASIC COMPONENTS OF THE MODEL

The Quark-Nova is an explosive transition from a neutron star (NS) to quark star (QS) (Ouyed, Dey, & Dey 2002; Keränen&Ouyed 2003). The result is a partial ejection of the NS crust (Keränen, Ouyed, & Jaikumar 2005) that leads to two possible types of debris surrounding the compact remnant (i.e. the QS) depending on the QS’s birth period. In OLNII, we showed that if the QS is born slowly rotating, then the debris formed from the QN ejecta will be in co-rotation, which we argue is responsible for SGRs. In OLNII, we showed that for QS born with millisecond periods, the debris evolves into a Keplerian ring with applications to AXPs. Furthermore, RRATs are the result of late evolution of the Keplerian ring in our model (OLNIII). The interested reader is referred to these papers for more details. Below we give an overview of the salient features of the model in the case of a Keplerian ring before we apply our model to transient AXPs.

2.1. The quark star: magnetically aligned rotator

The QN compact remnant is a quark star in the Color-Flavor-Locked (CFL) phase, which due to its rigorously

electric neutrality (Rajagopal & Wilczek 2001) possesses no crust. Owing to the superconductivity of the CFL state, the star’s interior contains a lattice of vortices that confine the magnetic field (Ouyed et al. 2004). This interior configuration consequently forces the exterior field to align with the rotation axis (Ouyed et al. 2006; Niebergal et al. 2006).

2.2. The Keplerian ring

There are two critical radii in our model during the quiescent phase, the inner radius R_{in} , and the outer ring radius R_{out} . In most cases these radii will be expressed in units of 15 km thus assigned a subscript 15. The other 2 parameters related to the geometry of the ring are the ring’s solid angle divided by 4π at R_{in} and R_{out} namely, $f_{\text{in},\Omega} = H_{\text{ring,in}}/R_{\text{in}}$ and $f_{\text{out},\Omega} = H_{\text{ring,out}}/R_{\text{out}}$. The ring thickness in the z -direction can be shown to be $H_{\text{ring}} \sim 2.68 \text{ km} \rho_{\text{ring},9}^{1/6} R_{15}^{3/2}$ where $\rho_{\text{ring},9}$ is the ring’s density in units of 10^9 gm cm^{-3} . General relativistic (GR) effects are included in the factors $f_{\text{GR,QS}} = \sqrt{1 - R_{\text{Sch.}}/R_{\text{QS}}}$, $f_{\text{GR,in}} = \sqrt{1 - R_{\text{Sch.}}/R_{\text{in}}}$, $f_{\text{GR,out}} = \sqrt{1 - R_{\text{Sch.}}/R_{\text{out}}}$ while $f_{\text{GR,ring}} = 0.5(f_{\text{GR,in}} + f_{\text{GR,out}})$ with $R_{\text{Sch.}}$ being the star’s Schwarzschild radius. Unless otherwise specified, quantities such as luminosity, temperature, and area are local values. Values at infinity are obtained by using the relevant GR factors. Finally, the ring area which includes top, bottom and inner surfaces is $A_{\text{out}} = 2\pi(R_{\text{out}}^2 - R_{\text{in}}^2) + 4\pi R_{\text{in}} H_{\text{ring,in}} = 2\pi R_{\text{out}}^2 Y_{\text{out}}$ where $Y_{\text{out}} = 1 - (R_{\text{in}}/R_{\text{out}})^2 + 2(R_{\text{in}}/R_{\text{out}})^2 f_{\text{in},\Omega}$.

Here we are concerned with compact remnants born with millisecond periods. As shown in OLNII, the quark star is surrounded by iron-rich Keplerian debris we refer to as a ring. This Keplerian ring is described in detail in §2.1 and Appendix A in OLNII. Briefly, the ring is iron-rich, degenerate material (the ejected NS crust material) in Keplerian rotation around the QS. The ring expands vertically and radially in time to a structure depicted in Figure 3 with $R_{\text{in}} \sim 15$ km and $R_{\text{out}} \sim 25$ km (for these fiducial values the total area of the ring is $A_{\text{ring}} \sim 3000 \text{ km}^2$). The ring is subject to tidal fracture and is made up of large cylinders we refer to as “walls”. The mass and width of a wall are given in OLNII and are $m_w \sim 10^{-10} M_{\odot}$ and $\delta r_w \sim 400 \text{ cm} R_{\text{in},15}^{3/2}$, respectively. The dipole field will not penetrate the degenerate part of the ring but only its inner most wall on timescales of a few hundred years (see §4). In general, at any given temperature the ring’s density below which the ring’s matter becomes non-degenerate is found by equating the ring temperature to its Fermi temperature; this defines the ring’s atmosphere which we discuss next.

2.3. The ring atmosphere

The atmosphere is characterized by its base density, scale height in the z -direction (vertical to the orbital plane), scale height in the radial direction (i.e. on the outer ring edge, R_{out} ; see appendix B in OLNII), and thermal speed,

$$\begin{aligned} \rho_{\text{atm}} &\simeq 460 \text{ gm cm}^{-3} T_{\text{keV}}^{3/2} & (1) \\ H_{\text{atm}}^z &\simeq 20.4 \text{ cm} \frac{T_{\text{keV}} R_{15}^{3/2}}{\mu_{3.3}} \end{aligned}$$

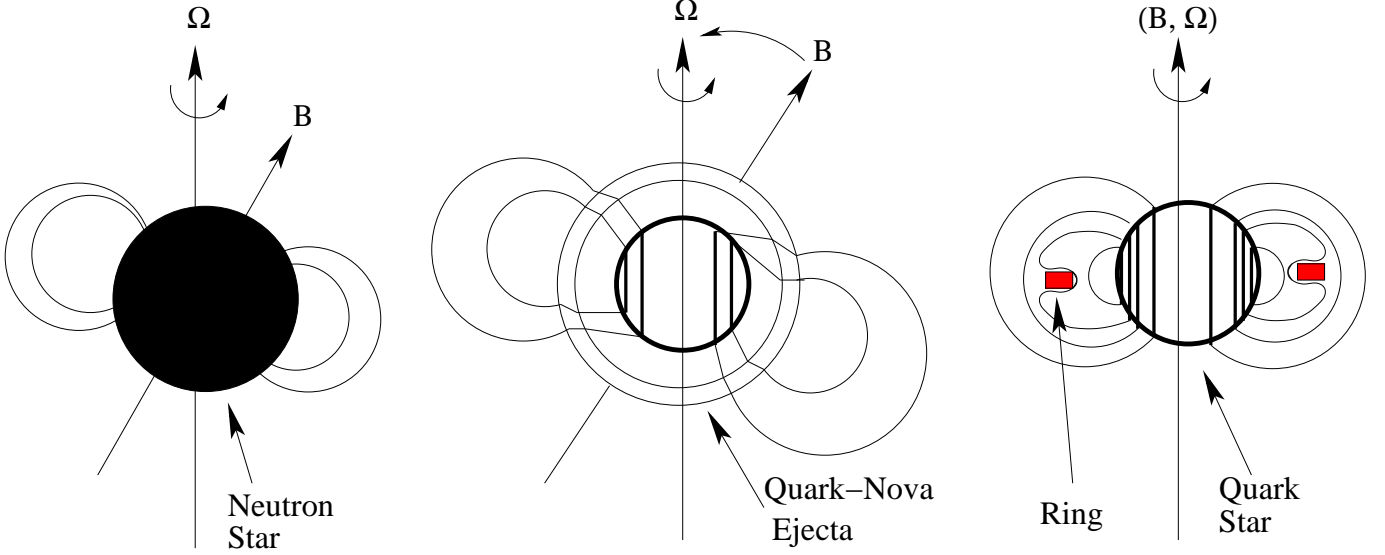


FIG. 1.— Illustrated here are the stages involved in the transition from a neutron star (NS) (inclined rotator) to a quark star (QS) (aligned rotator) in the Quark-Nova scenario. The collapse of the quark core induces an explosive NS-to-QS transition ejecting iron-rich degenerate crust material. The QS enters a superconductive phase confining the interior field to vortices, forcing the exterior field to align with the rotation axis (see Ouyed et al. 2004 for more details and Ouyed et al. 2006 for the related simulations). The iron-rich degenerate ejecta evolves into a Keplerian ring (a co-rotating ejecta is also possible depending on the NS period; see OLN1) surrounded by the dipole field.

$$H_{\text{atm,out}} \simeq 3.7 \text{ cm} \frac{T_{\text{keV}} R_{\text{out},15}^2}{\mu_{3.3}}$$

$$v_{\text{atm,th}} \simeq 9.4 \times 10^6 \text{ cm s}^{-1} \frac{T_{\text{keV}}^{-1/2}}{\mu_{3.3}^{1/2}},$$

where T_{keV} is the atmosphere temperature in keV, R_{15} is the radial position in units of 15 km, and $\mu_{3.3}$ is the mean molecular weight in units of 3.3 which represents a partially-ionized iron-rich atmosphere (see §3.2 in OLNII). The ring atmosphere's scale height in the z -direction is to be differentiated from that of the ring itself H_{ring} which as we have shown above is of the order of a few kilometers.

3. THE QUIESCENT PHASE IN OUR MODEL

3.1. The 2 blackbodies in quiescence

As discussed in OLN1 and OLNII, during the quiescent phase we have 2 blackbodies, one from the emission due to magnetic reconnection following vortex expulsion (the emission occurs just outside the star's surface). The resulting luminosity is

$$L_{\text{vortex}} \sim 2 \times 10^{34} \text{ erg s}^{-1} \eta_{\text{X},0.1} \dot{P}_{-11}^2, \quad (2)$$

with corresponding temperature,

$$T_{\text{vortex}} \simeq 0.2 \text{ keV} \eta_{\text{X},0.1}^{1/4} \frac{\dot{P}_{-11}^{1/2}}{R_{\text{QS},10}^{1/2}}, \quad (3)$$

where the period derivative is in units of $10^{-11} \text{ s s}^{-1}$, the star's radius in units of 10 km, and η_{X} is the efficiency parameter inherent in the conversion from magnetic energy to radiation in units of 0.1. The second BB results from reprocessing by the ring of the first BB's X-ray emission, $f_{\text{GR,QS}}^2 f_{\text{in},\Omega} L_{\text{vortex}} = f_{\text{GR,ring}}^2 A_{\text{ring}} \sigma T^4$. The ring-atmosphere system's temperature during quiescence is then, since $f_{\text{GR,QS}} \simeq f_{\text{GR,ring}}$,

$$T_{\text{q}} \sim 0.13 \text{ keV} \eta_{\text{X},0.1}^{1/4} \frac{\dot{P}_{-11}^{1/2}}{R_{\text{out},15}^{3/8} Y_{\text{out}}^{1/4}}, \quad (4)$$

where the subscript “q” stands for quiescent in contrast to the values during the bursting phase denoted by subscript “b”.

A correlation between the hot and cool BB has been noted by Nakagawa et al. (2007; see their figure 4), with $T_{\text{BB,H}}/T_{\text{BB,C}} \sim 2.5$. In our model, in quiescence the two blackbodies are associated with emission from vortex annihilation and the reprocessing of this emission by the ring. The resulting temperature ratio is

$$\frac{T_{\text{V}}}{T_{\text{q}}} = \left(\frac{A_{\text{ring}}}{f_{\text{out},\Omega} A_{\text{QS}}} \right)^{1/4} \sim 1.9 \left(\frac{R_{\text{out},25}}{R_{\text{QS},10}} \right)^{1/2}, \quad (5)$$

where $A_{\text{QS}} = 4\pi R_{\text{QS}}^2$ is the star's area. Since $\dot{P} \propto t^{-2/3}$ in our model (Niebergal et al. 2006), both BB temperatures during the quiescent phase evolve in time as $t^{-1/3}$.

3.2. Non-thermal X-ray emission

A strong non-thermal component has been observed by the International Gamma-Ray Astrophysics Laboratory (INTEGRAL) in several SGRs and AXPs (e.g. Nakagawa et al. 2007 and references therein). In our model, the vortex expulsion leads to magnetic field annihilation and creation of pairs. These pairs subsequently radiate synchrotron photons with energies $\nu_{\text{peak}} \sim 507 \text{ keV} \gamma_e^2 B_{14}$ where γ_e is the relativistic factor and the magnetic field is in units of 10^{14} G (see Ouyed et al. 2006). Synchrotron photons emitted downward towards the stellar surface are reprocessed into the blackbody described earlier. Thus the luminosity from vortex annihilation is split equally into thermal and power law (PL) components. This implies that the PL will decay with time as \dot{P}^2 (given in Niebergal et al. 2006; eq. 3). In some objects, the QN debris (co-rotating shell or Keplerian ring) can block much of the PL and BB caused by the vortex annihilation from the observer's line-of-sight. We note that the non-thermal component observed in AXPs and SGRs shows pulsation indicating that the emission

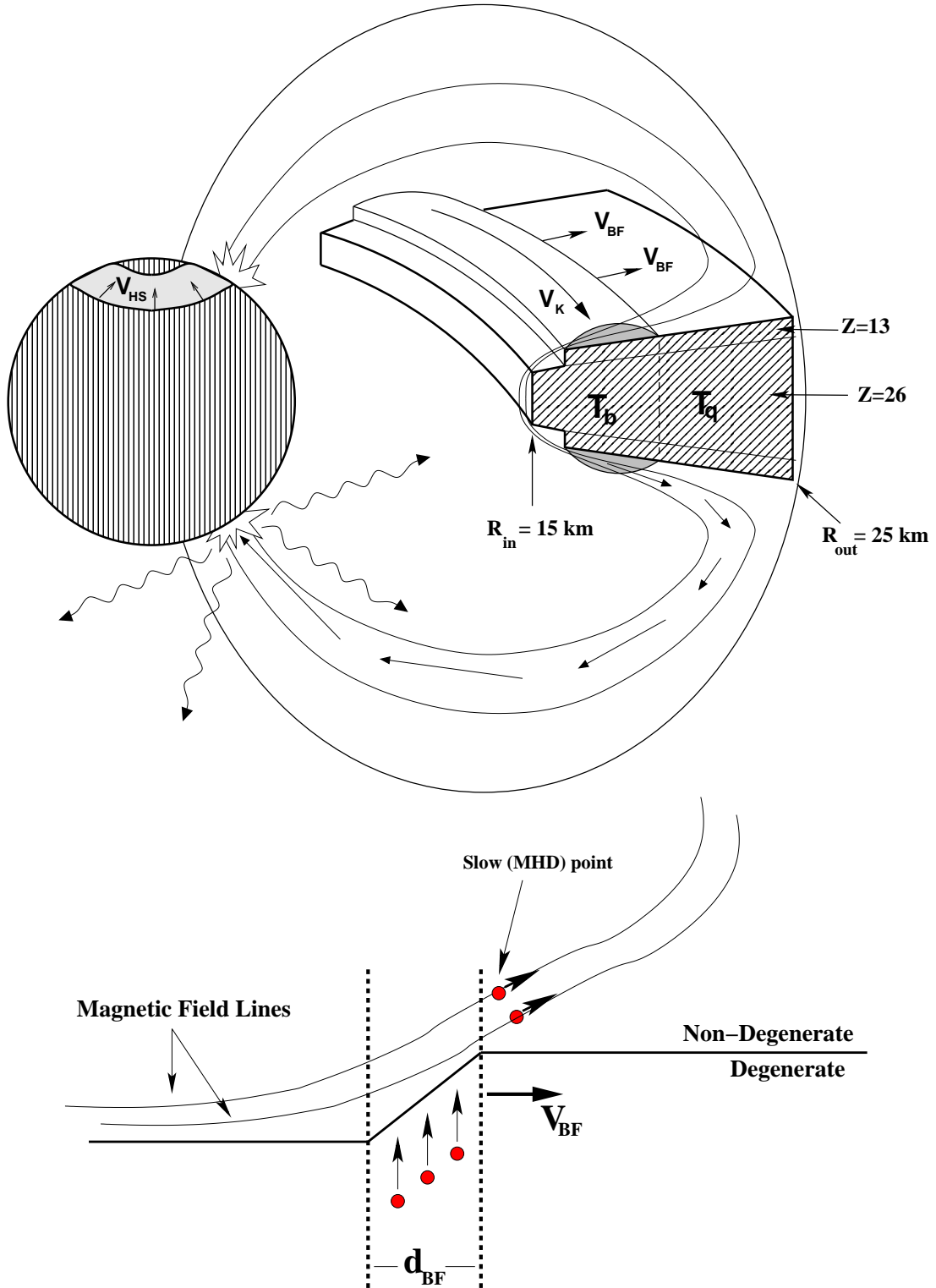


FIG. 2.— **The upper panel** illustrates the ring structure during outburst. Fiducial values of the ring inner radius (15 km) and outer radius (25 km) are shown; the ring's vertical scale height is a few kilometers (see §2.2; the figure is not to scale). The ring remains quiescent for hundreds of years until magnetic penetration of the inner edge (wall). Radiation from wall accretion leads to lighter dissociated nuclei ($Z \sim 13$) overlaying the deeper iron-rich ($Z = 26$) layers. This also heats the inner edge of the ring triggering a heat front (propagating via Bohm diffusion) at speed V_{BF} . As the Bohm Front (BF) moves from R_{in} to R_{out} , field lines detached from the BF. The footpoints on the quark star of the field lines threading the BF move poleward, decreasing the HS area. **The lower panel** illustrates motion and flow dynamics in the vicinity of the Bohm Front (BF). The solid line represents the transition to non-degenerate densities in the ring, ρ_{nd} , while d_{BF} is the radial width of the BF. As non-degenerate Keplerian material is expelled from the slow point, more Keplerian material is supplied from underneath (see Appendix B). Accretion shuts off once the magnetic field penetrates the non-degenerate Keplerian layer re-enforcing co-rotation.

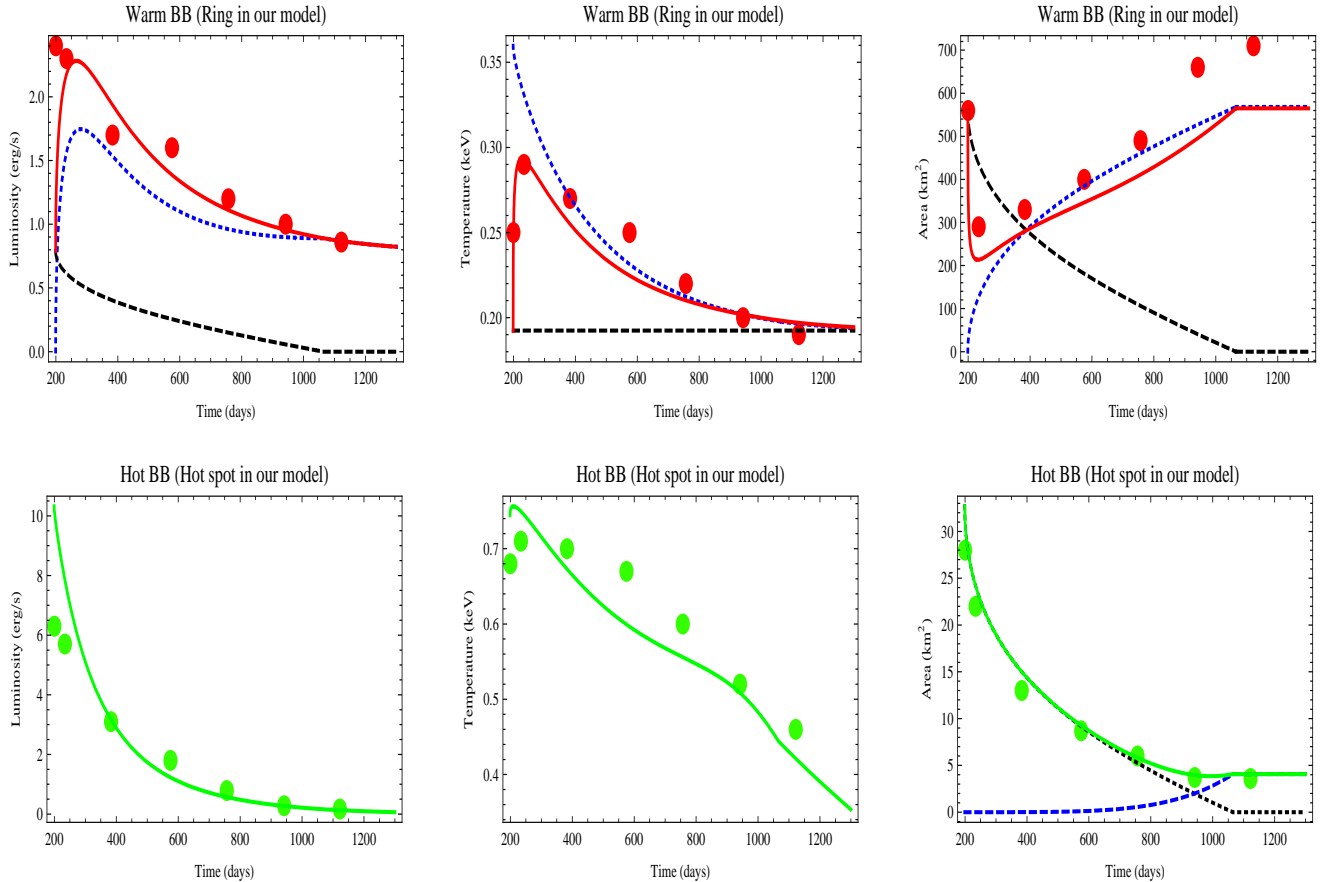


FIG. 3.— **Upper panels:** Model luminosity, temperature and area (curves) from one side of the ring as observed at infinity compared to observations (dots) of the warm component of XTE J1810–197. The dotted line is the contribution inward of the BF, the dashed is from outward of the BF, and the solid is the combined contribution (see text); **Lower panels:** Model luminosity, temperature and area (curves) from one pole as observed at infinity compared to observations (dots) of the hot component of XTE J1810–197. In the right-most panel the dotted line traces the shrinkage of the HS as the BF moves outward, the dashed line shows the late contribution from accretion induced by heating of the back side of the ring, and the solid is the combined contribution.

region is co-rotating with the star, consistent with our model.

4. BURSTING PHASE IN OUR MODEL

4.1. Wall accretion and change in mean molecular weight

As shown in OLNII (§4) the inner wall of the ring will be penetrated by the magnetic field on a time scale of hundreds of years². The energy released by the wall accretion is sufficient to dissociate a significant mass of iron nuclei in the ring into light nuclei (nuclei with $Z \sim 13$). As estimated in §4.4 in OLNII, for a typical wall mass $m_w \sim 10^{-10} M_\odot$, the number of dissociations following irradiation from wall accretion is $N_{13} \sim 10^{46} \zeta_{w,0.001} \eta_{0.1} m_{w,-10}$ where $\zeta_{w,0.001}$ is the dissociation efficiency in units of 0.001, and $\eta_{0.1}$ is the wall accretion efficiency in units of 0.1. Buoyancy drives the light ($Z \sim 13$) elements to the surface creating a two layer system as depicted in Figure 3. The depth of the $Z \sim 13$ can be estimated to be $H_{13} \sim 10^{-3} H_{\text{ring}}$; that is, or the order of a few meters.

² The ring’s atmosphere will be penetrated on much smaller timescales, $\sim 12 \text{ days } T_{\text{keV},0.1}^{5/2} R_{\text{in},15\text{km}}^3 \mu_{\text{atm},3.3}^{1/2}$, and is thus forced to co-rotate with the magnetic field; the temperature is in units of 0.1 keV representative of the quiescent phase.

The light nuclei diffuse into the ring atmosphere during burst, reducing the molecular weight from $\mu_q \sim 3.3$ to $\mu_b \sim 2.1\text{--}2.5$ (we adopt an average $\mu_b \sim 2.3$). Subsequent depletion of the $Z \sim 13$ nuclei by accretion leads to a return to an iron-rich atmosphere defined by $\mu_q \sim 3.3$:

$$\frac{1}{\mu} = \frac{1}{\mu_q} + \left(\frac{1}{\mu_b} - \frac{1}{\mu_q} \right) \exp^{-t/\tau_{13}}, \quad (6)$$

where τ_{13} is the depletion timescale. The depletion governs the exponential return of the system to its quiescent phase as discussed in the following sections; the depletion timescale is estimated in the Appendix (i.e. eq.(B3)) and is of order of a few years or less.

4.2. The 2 blackbodies during burst

Following wall accretion the inner parts of the ring are heated to $T_b > T_q$ leading to two other effects (besides the decrease in μ in the atmosphere): (i) a heat propagation outward along the ring’s atmosphere. The heat diffuses outward according to Bohm diffusion, thus introducing a critical radius in our model (during the bursting phase), $R_{\text{BF}} = R_{\text{in}} + \Delta r$, where Δr is the distance that the Bohm Front (BF) has travelled from R_{in} (see Appendix A); (ii) As the system (ring+atmosphere) is heated, the boundary between the non-degenerate atmosphere and degenerate ring material moves downwards

into higher density layers (see eq.(2) and Fig. 3). Thus Keplerian ring material is fed into the co-rotating atmosphere and is ejected as a magnetohydrodynamic wind (see Appendix B). The wind is then channeled onto the star with an accretion rate, $\dot{m}_{\text{acc.}}$, given by equation(B2).

The temperature of the inner ring is obtained by equating heating from accretion onto the quark star with blackbody cooling by the inner ring surface ($R < R_{\text{BF}}$); $f_{\text{GR,QS}}^2 f_{\text{BF},\Omega} L_{\text{acc.}} = f_{\text{GR,ring}}^2 A_{\text{BF}} \sigma T_{\text{b}}^4$ where $L_{\text{acc.}} = \eta \dot{m}_{\text{acc.}} c^2$ is the accretion luminosity, η the accretion efficiency, $f_{\text{BF},\Omega} = H_{\text{ring,BF}}/R_{\text{BF}}$, and the area created by the Bohm front is $A_{\text{BF}} = 2\pi(R_{\text{BF}}^2 - R_{\text{in}}^2) + 4\pi R_{\text{in}} H_{\text{ring,in}} = 2\pi R_{\text{BF}}^2 Y_{\text{BF}}$. Here $Y_{\text{BF}} = 1 - (R_{\text{in}}/R_{\text{BF}})^2 + 2(R_{\text{in}}/R_{\text{BF}})^2 f_{\text{in},\Omega}$. The resulting temperature is,

$$T_{\text{b}} \simeq 0.21 \text{ keV } \eta_{0.1} \zeta_{\text{sp},0.01} \frac{R_{\text{BF},15}}{\mu^{3/2} Y_{\text{BF}}} . \quad (7)$$

Here, $\zeta_{\text{sp},0.01}$ in units of 0.01, is a factor related to mass-loading at the slow MHD point as introduced in Appendix B. The approximation above is valid until late times when accretion ceases, so that T_{b} is no longer given by the accretion-cooling balance but rather settles to the quiescent temperature T_{q} . The outer ring's temperature is given by the quiescent temperature, eq.(4), until the heat front reaches it.

The accretion rate is then obtained by combining eq.(B2) with equation above to get

$$\dot{m}_{\text{acc.}} \sim 1.6 \times 10^{15} \text{ g s}^{-1} \eta_{0.1}^3 \zeta_{\text{sp},0.01}^4 \frac{R_{\text{BF},15}^{11/2} f_{\text{K}}(T_{\text{b}})}{\mu^6 Y_{\text{BF}}^3} . \quad (8)$$

The function $f_{\text{K}}(T_{\text{b}})$ is described in Appendix B and acts as a ‘‘valve’’ that shuts-off accretion after the heating front has passed. There is a fixed amount of Keplerian material at any radius that can be fed into an MHD wind and thus accreted onto the star. This is because of re-enforced co-rotation once the magnetic field penetrates the non-degenerate Keplerian layer effectively shutting off accretion (see Figure 2).

The natural connection between the BF outward expansion and the resulting hot spot (HS) on the star is illustrated in Figure 3. The corresponding HS luminosity is

$$L_{\text{acc.}} \sim 1.4 \times 10^{35} \text{ erg s}^{-1} \eta_{0.1}^4 \zeta_{\text{sp},0.01}^4 \frac{R_{\text{BF},15}^{11/2} f_{\text{K}}(T_{\text{b}})}{\mu^6 Y_{\text{BF}}^3} , \quad (9)$$

with a HS temperature

$$T_{\text{HS}} \sim 0.58 \text{ keV } \eta_{0.1} \zeta_{\text{sp},0.01} \frac{R_{\text{BF},15}^{11/8} f_{\text{K}}(T_{\text{b}})^{1/4}}{\mu^{3/2} Y_{\text{BF}}^{3/4} A_{\text{HS},120}^{1/4}} , \quad (10)$$

where the HS area, A_{HS} in units of 120 km², is derived in the Appendix (see eq. C1).

In summary, during the burst phase, the ring-atmosphere system consists of 2 BBs; the inner warmer part increasing in area at the Bohm diffusion rate and the outer cooler part decreasing in area. The hot BB in our model is provided by the HS which decreases in area as the BF propagates outwards.

The temperature ratio in the bursting phase case is then:

$$\frac{T_{\text{HS}}}{T_{\text{b}}} = \left(\frac{A_{\text{BF}}}{f_{\text{BF},\Omega} A_{\text{HS}}} \right)^{1/4} \sim 2.8 \left(\frac{R_{\text{out},25}}{R_{\text{QS},10}} \right)^{1/2} , \quad (11)$$

where we approximated $A_{\text{BF}} \sim A_{\text{ring}}/2$, $f_{\text{BF},\Omega} \sim f_{\text{out},\Omega}$, and $A_{\text{HS}} \sim 0.1 A_{\text{QS}}$ to get the numerical value. This is consistent with Figure 4 of Nakagawa et al. (2007). Our model predicts the temperature ratio during burst for a given object to be higher by a factor of ~ 1.5 than during quiescence. We expect a scatter in comparing different objects mainly caused by variations in R_{out} .

Overall, during burst and quiescence, the cool BB (from the co-rotating shell or Keplerian ring) arises from reprocessing radiation of the hot BB from the star (either vortex annihilation or accretion HS). We suggest, the relations in Figure 6 in Nakagawa et al. (2007) can be explained in the context of reprocessing during both quiescence and burst.

4.3. Non-thermal X-ray emission

The accreting material releases gravitational (~ 100 MeV per baryon) plus conversion energy (~ 50 MeV per baryon) which results in copious pair production. The pair generation mechanism is linked to complex radiative and collisional processes. Similar to the quiescent phase, the mildly relativistic pairs emit synchrotron photons in the strong magnetic field with energies up to a few hundred keV. Here as well downward emitted photons are reprocessed into thermal emission resulting in about equal contributions to thermal and non-thermal luminosities from the HS. For 4U 0142+614 (figure 3 of Nakagawa et al. 2007), one finds a power law luminosity of $\sim 5 \times 10^{35} (d/9 \text{ kpc})^2 \text{ erg s}^{-1}$. This agrees with the estimate based on our model $\sim 0.5 \times L_{\text{HS}}$, with L_{HS} given by equation (9).

Although difficult to differentiate observationally, during the bursting era, both PL emissions from the HS and from the vortex expulsion co-exist. However the PL from vortex expulsion becomes negligible as the source ages and \dot{P} decreases. For example, for 4U 0142+614 with $\dot{P}_{-11} \sim 0.2$, the PL from vortex expulsion is $0.5 \times L_{\text{vortex}} \sim 4 \times 10^{32} \text{ erg s}^{-1}$ which is dwarfed by the PL from the HS.

4.4. Application to XTE J1810–197

The upper panels in Figure 3 compares the time evolution of the ring's luminosity, temperature and area in our model to the observed warm BB in XTE J1810–197. In our model the luminosity from the inner part of the ring is $L_{\text{BF}} = A_{\text{BF}} \sigma T_{\text{b}}^4$ while the outer part gives $L_{\text{out}} = A_{\text{out}} \sigma T_{\text{q}}^4$ with $A_{\text{out}} = 2\pi(R_{\text{out}}^2 - R_{\text{BF}}^2)$. The total luminosity from the ring during burst is $L_{\text{ring,b}} = L_{\text{BF}} + L_{\text{out}}$ while the corresponding effective area and temperature were derived by weighting over luminosity, $A_{\text{ring,eff.}} = (A_{\text{BF}} L_{\text{BF}} + A_{\text{out}} L_{\text{out}})/L_{\text{ring,b}}$ and $T_{\text{ring,eff.}} = (T_{\text{b}} L_{\text{BF}} + T_{\text{q}} L_{\text{out}})/L_{\text{ring,b}}$.

The lower panels in Figure 3 compare the time evolution of the HS's luminosity, temperature and area in our model to the observed hot BB in XTE J1810–197. In this case, only one component comes into play, the accretion luminosity $L_{\text{acc.}}$. However, as the BF gets closer to R_{out} the back side of the ring is heated resulting in additional accretion by the same mechanism (i.e. eating into Keplerian material in the radial direction this time) and additional area on the polar cap defined by the field lines connecting the back side of the ring to the star (see Figure 2). The resulting area is $A_{\text{HS}} + A_{\text{edge}}$

and temperature $(L_{\text{acc.}}/(\sigma(A_{\text{HS}} + A_{\text{edge}})))^{1/4}$.

The fits to XTE J1810–197 data were obtained for the following set of parameters:

$$\begin{aligned} R_{\text{in}} &= 23.5 \text{ km} \\ R_{\text{out}} &= 26.5 \text{ km} , \end{aligned} \quad (12)$$

and by slightly adjusting the mass-load at the slow MHD point so that $\zeta_{\text{sp}} = 0.02$ (see discussion following eq.(B1)). The other parameters were kept to their fiducial values including the star’s parameters $R_{\text{QS}} = 10 \text{ km}$, $M_{\text{QS}} = 1.4M_{\odot}$. The star’s magnetic field is given by $B_{\text{QS}} = \sqrt{3\kappa P\dot{P}}$ (with $\kappa = 8.8 \times 10^{38} \text{ G}^2 \text{ s}^{-1}$ as given in eq.(10) in OLNIII).

Assuming that XTE J1810–197 has experienced a few bursting events, using equation (A.7) in OLNII, the ring would have spread to no more than $(\Delta r)_{\text{t}} \sim 8 \text{ km}$ if the system’s temperature during quiescence remained on average $\sim 0.1 \text{ keV}$. This is consistent with $(R_{\text{out}} - R_{\text{in}})$ found from fits to the XTE J1810–197 data thus providing a self-consistency check on our model. This also confirms our overall findings in previous work (OLNI, OLNII and OLNIII) that the ring should be a few kilometers in width after a few hundred years.

4.5. Application to 1E 1547.0–5408

In its bursting phase, this source was fitted with a $T \sim 0.5 \text{ keV}$ hot BB with $L_{\text{BB}} \sim 1.3 \times 10^{35} (d/9 \text{ kpc})^2 \text{ erg s}^{-1}$ and a corresponding area decreasing from 180 km^2 in June 2007 to 96 km^2 in August 2007 (see Halpern et al. 2008). During the quiescent phase, $L_{\text{BB}} \sim 10^{34} (d/9 \text{ kpc})^2 \text{ erg s}^{-1}$, $T_{\text{BB}} \sim 0.4 \text{ keV}$ and $A_{\text{BB}} \sim 36 \text{ km}^2$ (see Table 1 in Halpern et al. 2008).

This source has not been as well sampled as was XTE J1810–197. Nevertheless, in our model, high BB temperatures during the quiescent phase are suggestive of a more compact ring which is closer to the star (see eq.(4)). In our model, such a small and compact ring could have been a consequence of a smaller amount of crust material ejected during the QN (see eq.(2) in OLNII). For example, $R_{\text{out}} = 15 \text{ km}$ and $R_{\text{in}} = 13 \text{ km}$, which implies $Y_{\text{out}} \sim Y_{\text{BF}} \sim 0.117$, inserted in eq.(4) gives $T_{\text{q}} \sim 0.35 \text{ keV}$; we take $\dot{P}_{-11} \sim 2 \text{ s s}^{-1}$ for this source. The ring’s burst epoch temperature is then $\sim 0.48 \text{ keV}$ with a corresponding peak luminosity from eq.(9) of $L_{\text{acc.}} \sim 4.8 \times 10^{35} \text{ erg s}^{-1}$ for $\mu_{\text{b}} = 2.4$. This is close to the $\sim 1.3 \times 10^{35} (d/9 \text{ kpc})^2 \text{ erg s}^{-1}$ measured in June–July 2007 (the peak of the outburst was not observed and could have been higher than this). The initial area of the HS is given by equation (C1) and is estimated to be $\sim 80 \text{ km}^2$ using $R_{\text{in}} = 13 \text{ km}$ and $R_{\text{out}} = 15 \text{ km}$. Finally, in the case of 1E 1547.0–5408 there seems to be hints of an aligned rotator from its small X-ray pulsed fraction and its relatively broad radio pulse. In our model, the QN compact remnant (the QS) is born as an aligned rotator due to the vortex confinement of magnetic field (see Figure 1).

5. THE RADIO EMISSION IN OUR MODEL

5.1. Magnetic reconnection and bubble generation

After penetration, the magnetic field lines inside the wall (inner ring) are dragged by the Keplerian shear generating a toroidal magnetic field, B_{ϕ} . Continuous reconnection events during the winding of the field lines

lead to X-point generation and emergence of closed magnetic bubbles; more concisely these magnetically confined plasma bubbles result from the Keplerian shear. A rough estimate of the number of bubbles that can be generated is

$$N_{\text{Bub.}} \sim \frac{V_{\text{w}}}{V_{\text{Bub.}}} \sim 8.3 \times 10^6 R_{\text{in},15}^{3/2} , \quad (13)$$

where the total reconnection volume is $V_{\text{w}} \sim 4\pi R_{\text{in}} H_{\text{ring,in}} \delta r_{\text{w}}$ and $V_{\text{Bub.}} \sim (4\pi/3) \delta r_{\text{w}}^3$. The mass of a given bubble is thus $m_{\text{Bub.}} \sim (4\pi/3) \delta r_{\text{w}}^3 \rho_{\text{atm.,w}}$ where the plasma confined by the bubbles has a density $\rho_{\text{atm.,w}} \simeq 460 T_{\text{w,keV}}^{3/2} \sim 3600 \text{ gm cm}^{-3}$; the wall temperature immediately following burst is $T_{\text{w}} \sim 4 \text{ keV}$ (see §4.3 in OLNII).

5.2. Delay between the X-ray and radio emission

A closed magnetic bubble, confined by the dipole field, moves radially outwards at a rate given by $dr/dt = v_{\text{A}}$ where $v_{\text{A}} = B/\sqrt{4\pi\rho_{\text{Bub.}}}$ is the Alfvén speed and $\rho_{\text{Bub.}}$ the density of the plasma confined inside the bubble is taken to be $\rho_{\text{Bub.}} \simeq \rho_{\text{atm.}} (R_{\text{in}}/r)^{\alpha}$. The outward migration process, through the dipole field, is illustrated in Figure 4.

The time it takes the magnetic bubbles to reach the light cylinder (lc) at $R_{\text{lc}} = c/\Omega$ (at which point they start dissipating) is

$$t_{\text{delay}} \sim \frac{1}{4 - \frac{\alpha}{2}} \left(\frac{R_0}{c} \right) \left(\frac{R_{\text{lc}}}{R_0} \right)^{4 - \frac{\alpha}{2}} , \quad (14)$$

where $R_0 \sim 45 \text{ km} \left(B_{\text{QS},14} / T_{\text{atm,keV}}^{5/4} \right)^{1/(3-\alpha/2)}$ is the radius beyond which the Alfvén speed becomes sub-relativistic so that $v_{\text{A}} = c(R_0/r)^{3-\alpha/2}$. The star’s magnetic field $B_{\text{QS},14}$ is in units of 10^{14} G .

For example for $\alpha = 1$ which we adopt as our fiducial value (for which $R_0 \sim 100 \text{ km}$), we get

$$t_{\text{delay}} \sim 2 \text{ yrs } P_5^{7/2} , \quad (15)$$

where the period is given in units of 5 seconds. As they slow down while flowing towards the lc the bubbles will pile-up. This implies a delay between the X-ray outburst following wall accretion and the peak of radio emission in our model. Thus, following the peak of the X-ray outburst for XTE J1810–197 (with $P \simeq 5.54 \text{ s}$ and $R_{\text{in}} \sim 23 \text{ km}$) and 1E 1547.0–5408 (with $P \simeq 2 \text{ s}$ and $R_{\text{in}} \sim 13 \text{ km}$), we expect a corresponding radio peak emission to occur with a delay of $\sim 2.8 \text{ yrs}$ and $\sim 1 \text{ month}$ respectively.

5.3. Duration and luminosity

For a homologous expansion of the bubbles, a given bubble would increase in size as $\delta r_{\text{Bub.}} \sim \delta r_{\text{w}} (r/R_{\text{in}})$. By the time it reaches the lc, a given bubble would have increased in size from $\delta r_{\text{w}} \sim 400 \text{ cm}$ to about $R_{\text{Bub.}} \sim 63.5 \text{ km } R_{\text{in},15}^{1/2} P_5$. The bubble starts to dissipate as it “touches” the lc and slowly crosses it. It would take $t_{\text{Bub.,dis.}} \sim R_{\text{Bub.}}/v_{\text{A,lc}}$ for a given bubble to cross the lc (and fully dissipate) where $v_{\text{A,lc}}$ is the speed at which the bubble crosses the lc. For $\alpha = 1$, $v_{\text{A,lc}} \sim 107.4 \text{ cm s}^{-1} P_5^{-5/2}$ so that

$$t_{\text{Bub.,dis.}} \sim 0.7 \text{ days } R_{\text{in},15}^{1/2} P_5^{7/2} . \quad (16)$$

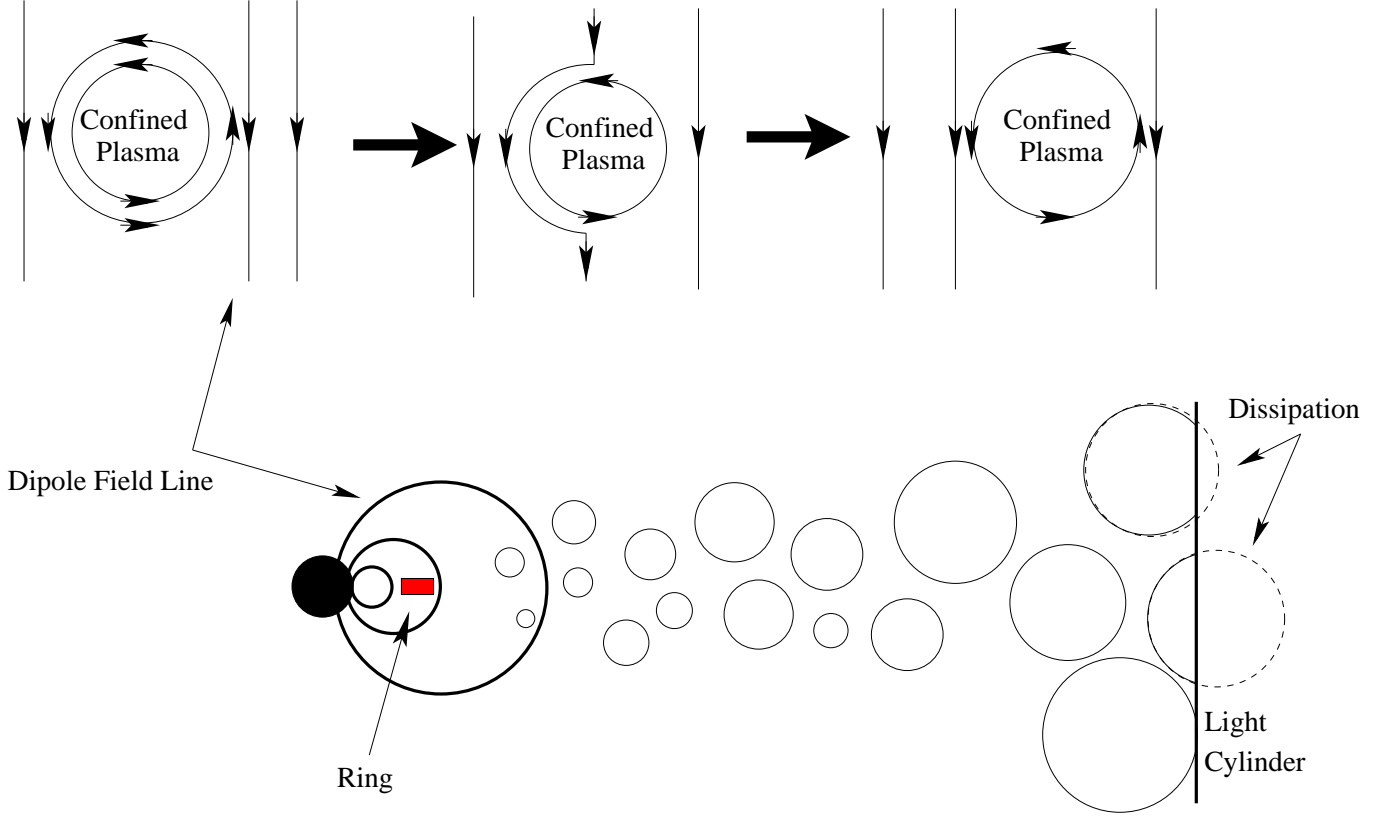


FIG. 4.— Keplerian shear during wall accretion leads to X-point reconnection which in turn causes the generation of closed magnetic loops, or “bubbles”. In our model, these magnetic bubbles are responsible for the radio emission seen in some AXPs. The top panel illustrates the outward migration of a bubble through the surrounding magnetic field. The lower diagram shows the overall pattern of bubble migration (i.e. magnetic buoyancy) and expansion that leads to pile up near the light cylinder. The bubbles dissipate as they cross the light cylinder leading to the radio emission (see text for details).

The duration of the radio emission in our model can then be estimated to be

$$t_{\text{radio}} \simeq \sqrt{N_{\text{Bub.}}} \times t_{\text{Bub.,dis.}} \sim 5.4 \text{ yrs } R_{\text{in},15}^{5/4} P_5^{7/2}. \quad (17)$$

In our model then, the radio emission would last about ~ 13 yrs for XTE J1810–197 and ~ 100 days for 1E 1547.0–5408. A more detailed estimate would require better knowledge of the velocity distribution of the bubbles, and a better evaluation of the expansion index, α .

Following penetration of the wall, in OLNII we showed that the twisted poloidal field $B_p = B_{\text{QS}}(R_{\text{QS}}/R_{\text{in}})^3$ acquires a toroidal component $B_\phi \sim B_p$. This toroidal component is partly stored in the magnetic bubbles which later dissipate at the lc. The radio luminosity is then given as

$$L_{\text{radio}} \simeq \eta_{\text{R}} \frac{B_\phi^2 V_{\text{w}}}{8\pi t_{\text{radio}}} \sim 4.5 \times 10^{31} \text{ erg s}^{-1} \frac{\eta_{\text{R},0.01} B_{\text{QS},14}^2}{R_{\text{in},15}^{13/4} P_5^{7/2}}, \quad (18)$$

where $\eta_{\text{R},0.01}$ is the reconnection efficiency we take to be of the order of 1% (e.g. Ouyed et al. 2006). For XTE J1810–197 this gives $L_{\text{radio}} \sim 7.3 \times 10^{30} \text{ erg s}^{-1}$ while for 1E 1547.0–5408 we get $L_{\text{radio}} \sim 10^{33} \text{ erg s}^{-1}$.

5.4. Pulse duration and shape

The total number of bubbles piling up at the lc, and crossing it, at any given time is $N_{\text{Bub.,lc}} \sim n_{\text{Bub.}} \times 4\pi R_{\text{lc}}^2 \times (2R_{\text{Bub.}}) \sim 1.3 \times 10^4 R_{\text{in},15}^2$ where the bubbles density is

$n_{\text{Bub.}} \sim N_{\text{Bub.}}/(4\pi R_{\text{lc}}^3/3)$. Because of co-rotation each bubble emits a radio pulse of duration $\simeq 2R_{\text{Bub.,lc}}/c \sim 0.4 \text{ ms } R_{\text{in},15}^{1/2} P_5$. This gives an averaged pulse duration $\sqrt{N_{\text{Bub.,lc}}} \times (2R_{\text{Bub.,lc}}/c)$, or,

$$\Delta t_{\text{pulse}} \sim 50 \text{ ms } R_{\text{in},15}^{3/2} P_5. \quad (19)$$

For XTE J1810–159, this gives an average pulse duration of 0.11 seconds in accordance with observations. For 1E 1547.0–5408 it is ~ 20 ms in our model.

5.5. The flat spectrum

As they cross the lc, the bubbles will dissipate by braking up into smaller bubbles while driving complex, non-linear reconnection events. Particle in Cell simulations of X-point reconnection events in a pair plasma have shown that highly variable radio emission, with an extremely flat spectrum ($s \sim -0.17$) is a natural outcome with pairs accelerated to Lorentz factors of up to ~ 70 (e.g. Figure 2 in Jaroschek et al. 2004). The flat spectrum is observed up to the cutoff frequency at ~ 100 GHz (e.g. Figure 4 in Jaroschek et al. 2004). These simulations show that the highly dynamic non-linear evolution of thin current sheets serve as the fundamental plasma scenario to obtain a flat synchrotron power spectra in pair-dominated environments. The emitted synchrotron emission is highly linearly polarized, with spectral polarization varying from $> 50\%$ around 1 GHz and up to 80% or higher at higher frequencies.

If pair generation regions exist in the vicinity of the lc then, when combined with magnetic reconnection events from bubble dissipation, it would offer a natural explanation for the observed flat spectrum. This could also help account for the prevalence of emission at a particular rotation phase (see fig. 2 in Camilo et al. Nature) which implies that the co-rotating bubbles must preferentially dissipate at a particular co-rotating longitude. It might also be the case that there exist a small non-uniformity at the light cylinder, caused by feedback from pairs produced by bubble dissipation mechanism itself.

5.6. Torques during radio emission

As each bubble expands toward the light cylinder it exerts a torque $\tau_{\text{Bub.}} = \Omega \times dI_{\text{Bub.}}/dt = 2\Omega m_{\text{Bub.}}rv_A$ where $I_{\text{Bub.}} = m_{\text{Bub.}}r^2$ is the moment of inertia of a bubble at a radius r from the star. The total torque exerted, $\tau = N_{\text{Bub.}}\tau_{\text{Bub.}}$, is then

$$\tau \sim 8.8 \times 10^{32} \text{ dyn cm} \frac{R_{\text{in},15}^6}{P_5} t_{\text{days}}^{-3/7}. \quad (20)$$

The corresponding frequency derivative, $\dot{\nu} = -\tau/(2\pi I_{\text{QS}})$ with $I_{\text{QS}} \sim 10^{45} \text{ g cm}^2$ for the star, is

$$\dot{\nu} \sim -1.4 \times 10^{-13} \text{ s}^{-2} \frac{R_{\text{in},15}^6}{P_5 I_{\text{QS},45}} t_{\text{days}}^{-3/7}. \quad (21)$$

This gives $\dot{\nu} \sim -1.9 \times 10^{-12} \text{ s}^{-2}$ and $\dot{\nu} \sim -10^{-13} \text{ s}^{-2}$ for XTE J1810–197 and 1E 1547.0–5408, respectively, which is of the right order of magnitude compared to what is observed. In our model, the torque decreases in time (as the X-ray decreases) in accordance with what has been observed in the case of XTE J1810–197 (Camilo et al. 2007c). However, for 1E 1547.0–5408, the torque increased in time as the X-ray flux decreased: this may be a consequence of a different dependency of the Alfvén speed in radius r in this system (i.e. $\tau \propto rv_A$) as to make the torque increase with radius.

6. DISCUSSION

6.1. Transient versus normal AXPs in our model

The 2 sources studied here are termed transients in the sense that in quiescence their measured temperatures are as low as those of some ordinary young neutron stars. Only during their bursting phase that their bolometric luminosity becomes comparable to that of a typical AXP in quiescence (i.e. a bolometric luminosity of $\sim 10^{35} \text{ erg s}^{-1}$). From approximate outburst time, the estimated initial bolometric luminosities for the two transients are $\sim 2 \times 10^{35} d_{3.3}^2 \text{ erg s}^{-1}$. Here we suggest the difference can be attributed to a difference in the magnetic field geometry at the outer ring’s edge between transients and regular AXPs.

In our model, the magnetic field decay from vortex expulsion implies that magnetic field lines deflate radially inwards³ while maintaining the dipolar configuration. At the same time the ring’s outer edge expands radially (see OLNII). This leads to a configuration where the magnetic field lines at the outer edge are favorable for thermal accretion during quiescence (as compared to

an MHD wind which requires Keplerian material; during bursting Keplerian material is fed to the atmosphere but we are only concerned with the quiescent phase here). As illustrated in Figure 5, in the early (i.e. small period) stages of a given source the magnetic field configuration is not favorable for accretion from the edge during quiescence. Thus, a transient AXP quiescent phase is dominated by X-ray emission from vortex expulsion only ($L_{\text{X,vortex}} \simeq 2 \times 10^{34} \dot{P}_{-11} \text{ erg s}^{-1}$) with the source continuing to evolve along the vortex band (see Figure 2 in OLNIII). On the other hand, a typical AXP (older ring-bearing source) quiescent phase is dominated by emission from the HS induced by accretion from the outer edge of the ring with $L_{\text{acc.}}$ given by eq.(9). These will evolve horizontally (at constant $L_{\text{HS}} \sim 10^{35} \text{ erg s}^{-1}$) as discussed in OLNII (see Figure 2 in OLNIII).

6.2. Birthrate

In our model, a QS-ring system experiences an X-ray/radio outburst every few hundred years⁴. Since we have observed 2 in a few years, located at distances of 3 to 9 kpc away (meaning we see about 30% of them), it is suggestive of a rate of 1 per year for the whole galaxy. This implies a total population of $(1/\text{yr}) \times 100 \text{ yrs} \sim 100$ in the galaxy. Since the ring will be consumed on a timescale of $\sim 10^4\text{--}10^5$ years (see eq. 5 in OLNIII) this gives a birthrate of (1 per 1000 years) to (1 per 100 years). Within uncertainties, the birth rate of transient AXPs derived above is consistent with the expected birthrate of AXPs ($\sim 1/300 \text{ yrs}$; Gill&Heyl 2007; Leahy&Ouyed 2007). As we argued in the previous section, in our model transient AXPs evolve into typical AXPs thus sharing the same birthrate.

6.3. Model features and predictions

The general predictions, starting with the X-ray emission, in our model are:

- **During X-ray Burst:** Since the accreted material in our model consists mostly of dissociated iron ($Z \sim 13$), we predict some sort of signatures either during channeling along the field line or on impact on the HS – maybe absorption lines or proton cyclotron lines ($\sim 0.14 B_{\text{QS},14} \text{ keV}$) from any of element in the Ne-to-S group (e.g. Ne, Al, Si). These signatures should be common for both transient and typical AXPs in our model.
- **During X-ray Quiescence:** When edge accretion occurs the signatures (e.g. absorption lines or proton cyclotron lines) should be from the $Z = 26$ rather than the $Z \sim 13$ nuclei.
- **X-ray variability :** During both the quiescent and bursting phases, X-rays from the ring+atmosphere system should be unpulsed and may carry the Keplerian signature via millisecond variability.

⁴ This is an upper limit since in our model, the radio outburst might not be seen if the period of the star is high enough to lead to long delays between the X-ray peak and radio peak. In other words, the older the system the more unlikely that the radio is observed.

³ Inside the star, the field lines expand outwards following the vortices.

Quiescent Phase

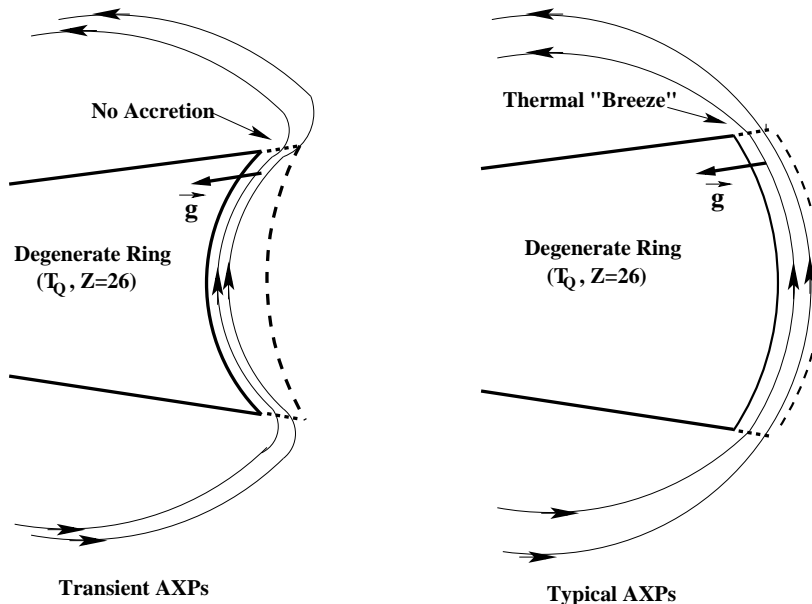


FIG. 5.— As the degenerate ring ages, its shape evolves because of viscous spreading. Shown in the left panel is the ring at an early age where its shape, calculated by hydrostatic equilibrium, is such that there is a cavity on the outer edge, for which the local acceleration of gravity (\vec{g}) impedes accretion. In our model, this is the state for a transient AXP, and its quiescent luminosity is dominated by vortex expulsion ($L_{X,\text{vortex}} \sim 2 \times 10^{34} \dot{P}_{-11} \text{ erg s}^{-1}$). In older sources (i.e. typical AXPs in our model) the outer edge assumes a convex configuration (see right diagram), where a thermal wind from the ring's outer edge is channeled by the magnetic field (i.e. not inhibited by \vec{g}); the corresponding luminosity during quiescence is then $L_{\text{HS}} \sim 10^{35} \text{ erg s}^{-1}$ (see OLNII).

- **Non-thermal X-ray emission** Pair production from vortex annihilation and/or from accretion onto the stellar surface results in PL synchrotron emission. Table 2, summarizes the different emission components for different objects in different states in our model. Compared to SGRs (see OLNII) and transient AXPs, typical AXPs acquire an additional BB and PL from the HS during quiescence. Only during bursting do transient AXPs acquire a HS. As for SGRs in our model, we recall (see OLNII) they are born with a co-rotating shell (i.e. non-Keplerian degenerate ring; see OLNII).

The general predictions for the radio emission are:

- **Radio Delay:** As can be seen from equation (15), the shorter the period of the star the smaller the delay, t_{delay} , between the X-ray burst and the radio emission. Interestingly, the 2 radio emitting AXPs so far are observed are those with the smallest period.
- **Radio Flux:** Furthermore, as can be seen from eq.(18), as P gets larger the radio following X-ray burst gets very faint making it more difficult to detect. Combined with long t_{delay} for large P , we argue these to be the reasons why radio is not observed following X-ray bursts in AXPs with higher (~ 10 s) period.
- **Radio Pulse Shape:** We predict changes in pulse shape and profiles on timescale of $\sim 0.7 R_{\text{in},15}^{1/2} P_5^{7/2}$ days (i.e. the time it takes a bubble to be con-

TABLE 1
THERMAL AND NON-THERMAL COMPONENTS IN OUR MODEL

Sources	Quiescent phase	Bursting phase
SGRs	2 BBs + 1 PL	3 BBs + 2 PLs
Transient AXPs	2 BBs + 1 PL	3 BBs + 2 PLs
Typical AXPs	3 BBs + 2 PLs	3 BBs + 2 PLs

The 2 PLs have the same index and different cut-offs and may be observationally indistinguishable.

sumed while crossing the lc; eq.(16)) for magnetars showing radio emissions..

Finally, we list specific predictions in our model in the case of XTE J1810–197:

- **XMM warm BB:** The XMM warm BB for XTE J1810–197 (ring+atmosphere system in our model) will evolve back to one single BB (ROSAT BB) with temperature T_q .
- **XMM hard BB:** The XMM hard BB (the accretion HS in our model) will disappear following burst (i.e. once the Bohm front reaches R_{out}). However, we expect edge effects to appear (e.g. flattening or even jump in the hot BB area; see last panel in Figure 3) just before accretion shuts off.
- **Radio Pulse Shape:** We predict changes in pulse shape and profiles on bubble dissipation timescale (eq.(16)) of ~ 1 day for XTE J1810–197 and ~ 40 minutes for 1E 1547.0–5408.

6.4. Further implications

There exist two aspects of our model that might provide some answers to fundamental issues in pulsar magnetospheres⁵. First, the source in the quark-nova model is born as an aligned rotator and secondly is the fact that here the degenerate ring, by Keplerian shear, is a natural source of plasma (carried by the bubbles to the l.c.) for the magnetosphere. Also, pairs are naturally supplied to the magnetosphere by vortex annihilation. This is left as an avenue for future investigation.

7. CONCLUSION

There are two fundamental components in our model for AXPs and transient AXPs namely, the QS and the Keplerian ring. In quiescence, vortex annihilation on the QS gives rise to thermal and non-thermal X-ray emission. The ring reprocesses the emission to give a second cooler BB emission component. Outburst is triggered by accretion of a small inner part of the ring (i.e. the wall). The

⁵ A disk model for X-ray emission from pulsars was considered by Michel & Dessler (1981). However, their disk is fundamentally different from our ring in that, where they hypothesize electron degenerate material (left over from a supernova), in our model the material is completely relativistic-degenerate (from a Quark-

two main consequences are production of light ($Z \sim 13$) nuclei and triggering MHD accretion onto the QS (yielding the HS). The interplay between the Bohm diffusion (i.e. R_{BF} term) and depletion of light nuclei (i.e. μ) gives rise to a rich behavior, necessary in order to account for the observed behavior of XTE J1810–197. Finally, one can ask if such a small Keplerian degenerate iron-rich ring could form around a neutron star. Ring formation when the neutron star is born appears implausible since a proto-neutron star is large compared to the ring size. After formation, there is no obvious mechanism to eject degenerate material unless a violent change of state, like a QN occurs.

This research is supported by grants from the Natural Science and Engineering Research Council of Canada (NSERC).

Nova). This difference has many consequences, the most notable are a more efficient accretion mechanism (conversion energy from the hadron to quark transition as well as gravitational energy is released), and a slower (viscous) spreading rate for the ring.

APPENDIX

A: THE BOHM DIFFUSION FRONT

The hot front propagates from the inner parts of the ring at a Bohm diffusion rate given by

$$\Delta r = \psi_{BF} \left(6.25 \times 10^{-4} \frac{T_{kev}}{B_{\perp,13}} \right)^{1/2} t^{1/2}, \quad (A1)$$

where $B_{\perp,13}$ is the magnetic field component perpendicular to the front motion in units of 10^{13} G. The parameter ψ_{BF} carries some uncertainty related to the fact that the above formula is semiempirical (i.e. the constant 1/16 in the original Bohm diffusion expression has no theoretical justification; see §5.10 in Chen 1984). This parameter is derived self-consistently in our model as explained in §B.2 below.

The ring geometry allows us to write $B_{\perp,13} \simeq \tan(\alpha_c) B_{BF,13}$ where to a first approximation $\tan(\alpha_c) = (H_{atm.,out}^z - H_{atm.,in}^z)/(R_{out} - R_{in})$ and $B_{BF} \simeq B_{av.} = B_{QS}(R_{QS}/R_{av.})^3$ where $R_{av.} = (R_{in} + R_{out})/2$; here $B_{QS} = \sqrt{3\kappa P\dot{P}}$ and R_{QS} are the star's magnetic field and radius, respectively. The temperature cancels out from eq.(A1) since $B_{\perp} \propto H_{atm.}^z \propto T_{kev}/\mu$ so that,

$$\Delta r \sim 10^{-2} \text{ km } \psi_{BF} \left(\frac{\mu_{3.3}}{B_{av.,13} R_{out,15}^{1/2}} \right)^{1/2} t_{days}^{1/2}. \quad (A2)$$

B: CENTRIFUGAL EJECTION AND CHANNЕLED ACCRETION

As the system (ring+atmosphere) is heated, the boundary between the non-degenerate atmosphere and the degenerate $Z \sim 13$ layer moves downwards into higher density layers (see eq.(2)). Thus Keplerian ring material is fed into the atmosphere and is ejected as a magnetohydrodynamic wind as outlined below.

Production of magneto-hydrodynamic (MHD) jets by non-degenerate Keplerian accretion disk has been established in the literature (Blandford&Payne 1982). It has been shown that the wind can be launched centrifugally if the field direction is inclined at an angle less than 60° to the radial direction. These conditions are easily met in our model so that the newly unveiled Keplerian material (following heating of the degenerate ring) finds itself threaded by the highly inclined magnetic field and is flung out centrifugally; the so-called “bead-on-wire” analogy. In this picture, the mass flux, \dot{m}_{wind} , is regulated by conditions (i.e. density) at the slow mode critical point. The ejected material is then channeled/accreted onto the star at a rate, $\dot{m}_{acc.} \sim \dot{m}_{wind}$,

$$\dot{m}_{acc} = 4\pi R_{BF} \zeta_{sp} (\rho_{atm.,b} H_{atm.,b}^z - \rho_{atm.,q} H_{atm.,q}^z) v_{atm,th}, \quad (B1)$$

where $(\rho_{atm.,b} H_{atm.,b} - \rho_{atm.,q} H_{atm.,q}) = \rho_{atm.,b} H_{atm.,b} \times f_K(T_b)$ describes the mass injected from the Keplerian ring into the atmosphere. The function $f_K(T_b) = 1 - T_q^{5/2}/T_b^{5/2}$ evolves from ~ 0.8 to zero as the non-degenerate Keplerian material is depleted and the system evolves back to its quiescent phase. In a sense it acts as a “valve” that shuts-off

accretion after the heating front has passed. The accretion rate can be recast to

$$\dot{m}_{\text{acc.}} = 1.77 \times 10^{17} \zeta_{\text{sp},0.01} \frac{T_{\text{b,keV}}^3 f_{\text{K}}(T_{\text{b}}) R_{\text{BF},15}^{5/2}}{\mu^{3/2}}. \quad (\text{B2})$$

The factor ζ_{sp} carries the uncertainty on the exact location of the slow MHD mode. We will adopt $\zeta_{\text{sp}} \sim 0.01$ as inferred from 2-dimensional and 3-dimensional MHD simulations of disk winds (Ouyed et al. 2003). The slow MHD point governs the mass loss rate. The degenerate ring responds by supplying mass at a rate $\dot{m}_{\text{BF}} \sim \rho_{\text{atm}} 2\pi R_{\text{BF}} d_{\text{BF}} v_{\perp}$ where v_{\perp} is the velocity of degenerate Keplerian material crossing the boundary to non-degeneracy⁶, and d_{BF} is the radial width of the BF as illustrated in Figure 2.

Accretion shut-off

MHD accretion shuts-off once the magnetic field has penetrated into the thin non-degenerate Keplerian layer re-enforcing co-rotation. The penetration timescale can be estimated from equation (16) in OLNII to be $\tau_{\text{B,K}} \sim 4 \text{ days } H_{\text{K,cm}}^2 / T_{\text{keV}}^{1/2}$ where the depth of the non-degenerate Keplerian layer $H_{\text{K}} \sim 10^{-3} H_{13} \sim 10^{-6} H_{\text{ring}}$ is in units of centimeters. The size (i.e. radial width) of the BF front is found from $d_{\text{BF}} = v_{\text{BF}} \tau_{\text{B,K}} \sim 10^3 \text{ cm}$ which is of the same order as the depth of the $Z \sim 13$ layer.

Depletion timescale of the $Z \sim 13$ nuclei

We recall that following wall accretion and subsequent irradiation of the ring, up to 10^{46} of iron nuclei are dissociated forming the $Z \sim 13$ layer. The depletion timescale is given by $\tau_{13} \sim m_{13} / \dot{m}_{\text{acc.}}$ where $m_{13} \sim N_{13} \times (13 m_{\text{H}})$. For typical values following wall accretion $\mu = \mu_{\text{b}} \sim 2.3$, $R_{\text{BF}} \sim R_{\text{in}}$, $Y_{\text{BF}} \sim 0.4$, and $\eta = 0.1$, we find

$$\tau_{13} \sim 1.4 \times 10^4 \text{ days } \frac{N_{13,46}}{\zeta_{\text{sp},0.01}^4}, \quad (\text{B3})$$

where $N_{13,46}$ is the total number of dissociated iron nuclei in units of 10^{46} (see §4.1).

We have already estimated the size of the BF region above which we found to be of the same order as the depth of the $Z \sim 13$ layer which implies that our scenario self-consistently leads to the accretion of most of the $Z \sim 13$ material during burst (i.e. during the time it takes the BF to comb the ring's surface). In other words, the depletion timescale can also be estimated from eq.(A2) by taking $\Delta r = (R_{\text{out}} - R_{\text{in}})$ and $\mu = \mu_{\text{b}} \sim 2.3$ to get

$$\tau_{13} \sim \frac{1.5 \times 10^4}{\psi_{\text{BF}}^2} \text{ days } (R_{\text{out}} - R_{\text{in}})_{\text{km}}^2 R_{\text{out},15}^{1/2} B_{\text{av.},13}, \quad (\text{B4})$$

where $(R_{\text{out}} - R_{\text{in}})$ is in units of kilometers. Equating the previous two equations we find

$$\psi_{\text{BF}} \sim \frac{\zeta_{\text{sp},0.01}^2 (R_{\text{out}} - R_{\text{in}})_{\text{km}} R_{\text{out},15}^{1/4} B_{\text{av.},13}^{1/2}}{N_{13,46}^{1/2}}, \quad (\text{B5})$$

which fine tunes the speed of the BF in our model (i.e. eq.(A2)).

C: RING-POLE INTERACTION: THE HOT SPOT

As illustrated in Figure 2, there is a direct link between the BF moving outward along the ring surface (increasing its area) while decreasing the area of the HS on the surface of the star. It is straightforward to show that the total HS area (both poles) is

$$A_{\text{HS}} = 4\pi R_{\text{QS}}^2 \times (\cos \beta_{\text{BF}} - \cos \beta_{\text{in}}), \quad (\text{C1})$$

where the angle β defines the colatitude (i.e. measured from the polar axis) on the star's surface where material channeled along a given field line lands. We approximate the field by a dipole configuration, giving us

$$\sin \beta = \left(\frac{R_{\text{QS}}}{R} \right)^{1/2} \sin \alpha, \quad (\text{C2})$$

where

$$\alpha = \frac{\pi}{2} - \arctan \frac{H_{\text{ring}}}{R}, \quad (\text{C3})$$

is the angle from the polar axis to the footpoint, at radial distance R , of the field line where the Keplerian material is loaded; $H_{\text{ring}} \sim 2.68 \text{ km } \rho_{\text{ring},9}^{1/6} R_{15}^{3/2}$ is the ring's vertical height as given in §2.2. For our fiducial values, $R_{\text{in}} = 15 \text{ km}$, $R_{\text{out}} = 25 \text{ km}$ and $R_{\text{QS}} = 10 \text{ km}$, we find $(\cos \beta_{\text{out}} - \cos \beta_{\text{in}}) \sim 0.192$ which gives an initial area of the HS at one pole of the order of $\sim 120 \text{ km}^2$.

REFERENCES

- Blandford, R. D., & Payne, D. G. 1982, MNRAS, 199, 883
 Camilo, F. et al., 2006, Nature, 442, 892
⁶ We recall that in the degenerate Keplerian disk, lower viscosity and conservation of angular momentum imply mass flows in the ring are along lines of constant angular momentum which is nearly vertical (i.e. z -direction; see Appendix A in OLNII). Thus as the non-degenerate Keplerian material is "sucked up" in the wind, more material is supplied almost vertically from the underlying Keplerian material.

- Camilo, F., Ransom, S. M., Halpern, J. P., & Reynolds, J. 2007a, *ApJ*, 666, L93
- Camilo, F., et al. 2007b, *ApJ*, 663, 497
- Camilo, F., et al. 2007c, *ApJ*, 669, 561
- Camilo, F., Reynolds, J., Johnston, S., Halpern, J. P., & Ransom, S. M. 2008, *ApJ*, 679, 681
- Gelfand, J. D., & Gaensler, B. M. 2007, *ApJ*, 667, 1111
- Gill, R., & Heyl, J. 2007, *MNRAS*, 381, 52
- Gotthelf, E. V., & Halpern, J. P. 2007, *Ap&SS*, 308, 79
- Halpern, J. P., & Gotthelf, E. V. 2005, *ApJ*, 618, 874
- Halpern, J. P., Gotthelf, E. V., Reynolds, J., Ransom, S. M., & Camilo, F. 2008, *ApJ*, 676, 1178
- Ibrahim A.I., Markwardt C.B., Swank J.H., et al., *ApJ*, 2004, 609, L21
- Jaroschek, C. H., Lesch, H., & Treumann, R. A. 2004, *ApJ*, 605, L9
- Kaspi, V. M. 2007, *Ap&SS*, 308, 1
- Keränen, P., & Ouyed, R. 2003, *A&A*, 407, L51
- Keränen, P., Ouyed, R., & Jaikumar, P. 2005, *ApJ*, 618, 485
- Leahy, D., & Ouyed, R. 2007, arXiv:0710.2114
- Leahy, D., & Ouyed, R. 2008, *MNRAS*, 387, 1193
- Michel, F. C., & Dessler, A. J. 1981, *ApJ*, 251, 654
- Nakagawa, Y. E., Yoshida, A., Yamaoka, K., & Shibasaki, N. 2007, arXiv:0710.3816
- Niebergal, B., Ouyed, R., & Leahy, D. 2006, *ApJ*, 646, L17
- Niebergal, B., Ouyed, R., & Leahy, D. 2007, *A&A*, 476, L5
- Ouyed, R., Dey, J., & Dey, M. 2002, *A&A*, 390, L39
- Ouyed, R., Clarke, D. A., & Pudritz, R. E. 2003, *ApJ*, 582, 292
- Ouyed, R., Elgarøy, Ø., Dahle, H., & Keränen, P. 2004, *A&A*, 420, 1025
- Ouyed, R., Niebergal, B., Dobler, W., & Leahy, D. 2006, *ApJ*, 653, 558
- Ouyed, R., Leahy, D., & Niebergal, B. 2007a, *A&A*, 473, 357 (OLNI)
- Ouyed, R., Leahy, D., & Niebergal, B. 2007b, *A&A*, 475, 63 (OLNII)
- Ouyed, R., Leahy, D., Niebergal, B., & Yue, Y. 2008, arXiv:0802.3929 (OLNIII)
- Rajagopal, K., & Wilczek, F. 2001, *Physical Review Letters*, 86, 3492
- Woods, P. M., & Thompson, C. 2006, *Compact stellar X-ray sources*, 547